PREFORMING OF MULTI-PLY NON-CRIMP FABRIC LAMINATES USING DOUBLE DIAPHRAGM FORMING

Guy D. Lawrence, Shuai Chen, Nicholas A. Warrior, Lee T. Harper*
*Corresponding author – lee.harper@nottingham.ac.uk

Composites Research Group, Faculty of Engineering, University of Nottingham, NG7 2RD, UK

Keywords: *NCF, forming, wrinkling, multi-ply, friction, automation*

ABSTRACT

Double diaphragm forming (DDF) is a cost effective, semi-automated method of producing non-crimp fabric (NCF) preforms for use in liquid composite moulding processes. It relies on vacuum-only generated forming forces and single-sided tooling to produce complex double-curved fabric preforms. However, the formation of wrinkles presents a significant barrier to the wider adoption of DDF, as they reduce the efficacy of the mechanical properties of the finished composite component. The fabric shear and bending deformation mechanisms that are responsible for generating these wrinkles are well understood for thin laminates constructed of only one or two plies, but the influence of inter-ply friction complicates matters, particularly for thicker preforms with higher ply counts.

This paper aims to characterise the bending and shear behaviours of multi-ply laminates using modified cantilever bend and bias extension tests respectively. It is demonstrated that the inter-ply friction increases both the bending and shear stiffnesses of a dry fibre preform, reducing its formability. A DDF case study is presented for an industrially relevant geometry, demonstrating the combined effect of the number of plies and the layup sequence on the formability of the preform.

1. INTRODUCTION

Double diaphragm forming (DDF) is a scalable, semi-automated process capable of producing multi-layer composite preforms through the use of vacuum pressure to generate uniform draping forces [1,2]. DDF employs the use of two deformable membranes, which are used to consolidate and therefore constrain multiple plies of composite material using a vacuum. A second, independent, hydrostatic vacuum is drawn beneath the diaphragm assembly, causing the preform stack to deep-draw and form over a male tool geometry. Whilst DDF has most commonly been used to form prepreg material [3,4], its application to binder-stabilised dry fabrics for use in liquid composite moulding processes is increasing due to the potential for low-cost mass manufacture. Forming of non-crimp fabrics (NCFs) is particularly attractive due to their stability when cutting and handling, producing highly repeatable preforms.

The formation of defects presents a significant challenge to the development of DDF for complex geometries for higher volume applications. Out-of-plane wrinkling, in-plane fibre buckling and poor fabric-tool conformity can reduce the mechanical properties of a finished NCF part by up to 70% [5]. Previous work investigating defect formation in DDF has typically focused on the forming on preforms constructed of only one or two plies [6–8]. The shear [9], bending [10] and friction [11,12] mechanisms that produce defects such as out-of-plane wrinkling and fibre buckling are well understood for thin preforms, but the additional constraints caused by an increasing number of plies are less well known. Inter-ply deformation mechanisms including friction and fabric compaction have a significant effect on the formability of a preform as the number of inter-ply interactions increases. Liang et al. [13] demonstrated that the bending stiffness of a multiply stack is greater than the sum of the bending stiffness of its individual plies, due to the inter-ply friction in the stack. It is necessary to take the contribution from the inter-ply friction into account when modelling the fabric bending behaviour. Previous work has shown that the inter-ply coefficient of friction is highly dependent on the applied normal load [11], which increases by up to 43% when vacuum pressure (1×10^5 Pa) is applied. Therefore, it is likely that the bending stiffness of a thick laminate during DDF processing is significantly higher than previously anticipated. In addition, increasing the inter-ply friction in the preform stack also constrains the shearing behaviour of individual plies, further reducing the formability for thick laminates.

This work aims to demonstrate how large frictional forces generated by an increased number of plies in a thick laminate can increase the bending stiffness and shear resistance of a fabric stack, reducing formability. This will be achieved using a combination of existing coupon-level characterisation methods and a component-level DDF demonstrator case study.

2. METHODOLOGY

2.1. MATERIALS

The NCF material used for the study is designated FCIM359 and was provided by Hexcel Reinforcements, Leicester, UK. FCIM359 is a pillar stitched biaxial carbon fibre NCF, as described in Table 1. All fabric samples used in this study were cut using an Assyst Bullmer XCUT automated single ply cutter to ensure repeatability, accuracy and to minimise sample preparation time for the large numbers of plies.

Table 1 - Material properties of FCIM359 [11].

Name	FCIM359
Supplier	Hexcel
Fabric type	Biaxial NCF
Areal weight	441gsm
Fabric thickness	0.4mm
Stitching	Polyester pillar stitch, 4.5mm spacing
Fibre	24k carbon tows
On-roll fabric orientation	Stitch 0°, fibre ±45°

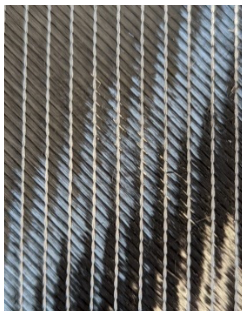

2.2. MULTI-PLY BENDING CHARACTERISATION

A revised cantilever bend test was used to characterise the non-linear bending stiffness of multi-ply laminates, following a proven test methodology [10,13,14]. To characterise the bending of multi-ply samples, low weight thread was looped around the fabric stack to inhibit separation of plies when bending, whilst continuing to allow inter-ply slip (Figure 1a). A Creaform HandyScan 3D Silver Series scanner was used to digitise the surface of the bending test sample in the form of XYZ point cloud data (Figure 1b). Only the central 10% of data points from each scan were used to produce a bending profile, reducing the influence of any unwanted twist or misalignment in the fabric. The bending moment versus specimen curvature curve was obtained by fitting a 6^{th} order polynomial to the data points for each sample.

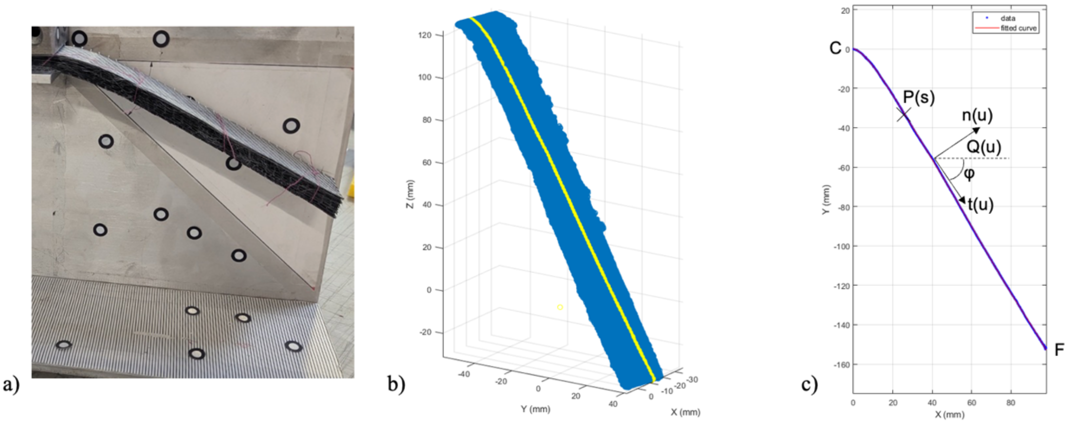

Figure 1a) Photo of 16-ply cantilever bend test setup with reflective reference points for 3D scanner. b) Digitised point cloud indicating the central region used for post-processing. c) Bending profile of a single ply sample, where C indicates the constrained end and F indicates the free end.

The bending moment versus curvature curves were calculated for each specimen using Equations 1-4 [14]:

$$\kappa = \frac{y''}{(1 + y'^2)^{\frac{3}{2}}} \tag{1}$$

$$L_B = \int_{X_C}^{X_F} \sqrt{1 + y'^2}\, dx \tag{2}$$

$$s(P) = \int_{X_C}^{X_P} \sqrt{1 + y'^2}\, dx \tag{3}$$

$$M(s) = W \int_{s}^{Lb} (u - s) \cos(\varphi)\, du \tag{4}$$

where κ is the curvature of the bending curve, L_b is the bending length of the curve (equivalent to the overhang length), s is the curvilinear abscissa, φ is the angle of the curve tangent to the horizontal, W is the specimen weight per unit length, and M is the bending moment per unit width of the specimen.

The subsequent bending moment versus curvature relationship can be described using Voce's model [15] as per Equation **Error! Reference source not found.**, where R_0 and R_{Inf} are fitting constants and κ_{lim} is the exponential saturation parameter.

$$M(\kappa) = (R_0 \cdot \kappa) + R_{Inf}(1 - \exp(1 - \frac{\kappa}{\kappa_{lim}})) \tag{5}$$

2.3. MULTI-PLY SHEAR CHARACTERISATION

A bias-extension test was selected to characterise the shear behaviour of a multi-ply laminate, as a compaction pressure normal to the fabric surface can be applied with a vacuum bag more easily than with a picture frame shear test. The bias extension test methodology is described extensively by Cao. et al [16]. To describe the shear behaviour of the fabric, a shear angle (γ) vs. shear force (F_{Sh}) curve was obtained for each experiment, calculated using Equations 6 and 7, where H and W are the height and width of a fabric sample, δ is the crosshead displacement, F is the crosshead load and F_{Sh} is the normalised shear force.

$$\gamma = 90 - 2\cos^{-1}\left(\frac{(H-W)+\delta}{\sqrt{2}(H-W)}\right) \tag{6}$$

$$F_{Sh}(\gamma) = \frac{1}{(2H-3W)\cos(\gamma)}\left(\left(\frac{H}{W}-1\right)F\left(\cos\left(\frac{\gamma}{2}\right)-\sin\left(\frac{\gamma}{2}\right)\right) - WF_{Sh}\left(\frac{\gamma}{2}\right)\cos\left(\frac{\gamma}{2}\right)\right) \tag{7}$$

To simulate the compaction pressures experienced during DDF, the fabric samples for the bias extension test were placed inside a vacuum bag sock (Figure 2). The force required to shear the sample and extend the vacuum bag can be described by Equation 8 [17], where F_d is the load required to extend the vacuum bag and F_f is the frictional force between the vacuum bag and the fabric sample:

$$F_{Sh} = F - F_d - F_f \tag{8}$$

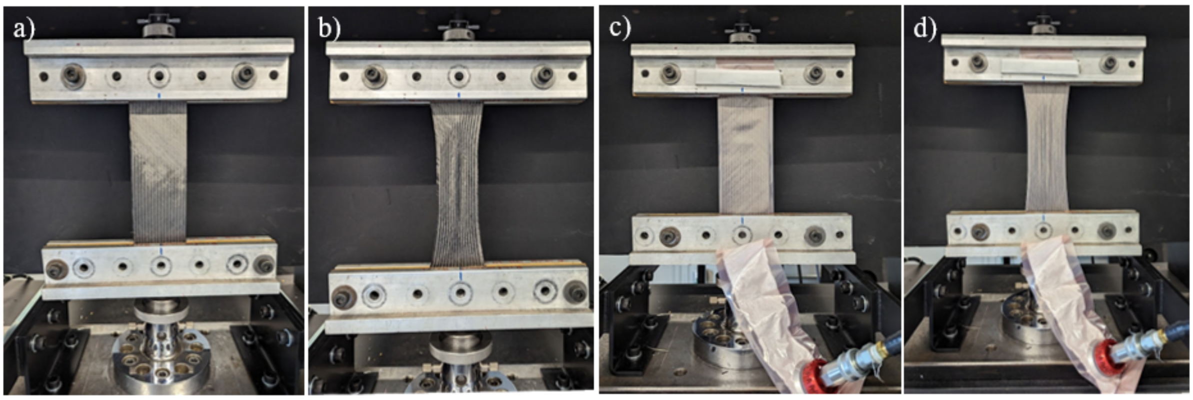

Figure 2 – Bias extension tests of a single ply of FCIM359. a) Pre-test, no vacuum. b) Post-shearing, no vacuum. c) Pre-test, induced vacuum. d) Post-shearing, induced vacuum.

Additional NCF plies were included in the bias extension test at a [0°/90°] orientation to investigate the influence of inter-ply friction on the intra-ply shear behaviour. These samples were shorter than the original [±45°] plies and so were unconstrained (i.e., not clamped at either end) to avoid the unwanted tensile contribution from the [0°/90°] fabric in the measured crosshead force. The layup sequence of the resulting fabric stack was varied to change the number of interfaces between samples of different orientations where sliding may occur.

2.4. EXPERIMENTAL FORMING METHODOLOGY

A laboratory-scale diaphragm forming machine, as shown in Figure 3a, was used to conduct experimental DDF work. Stretchlon® HT-350 was used for the diaphragm material, with dimensions of approximately 1.8m x 1.5m. The forming machine clamps the two diaphragms between three aluminium frames, which are then lowered into position over the male forming tool using four pneumatic cylinders.

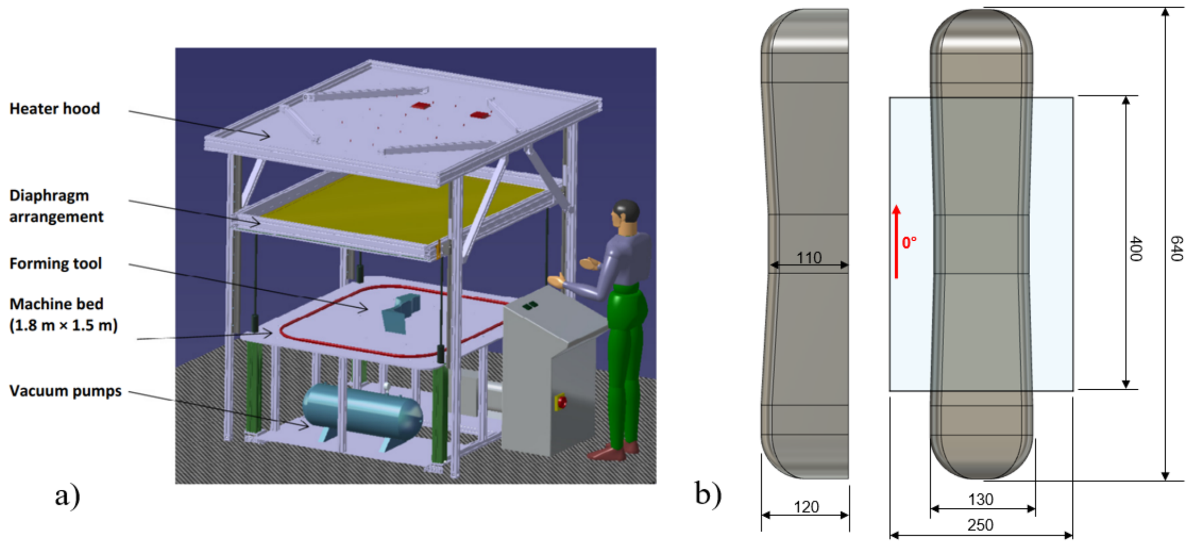

Figure 3a) Schematic of the diaphragm forming machine at the University of Nottingham, UK [9]. b) Geometry of male c-spar tool and fabric blank used for experimental study. (Dimensions in mm).

The male tool geometry used for the experimental work is displayed in Figure 3b, which is similar to the geometry used by Johnson et al. [18]. The c-spar was selected as it is representative of a typical aerospace wing spar component and contains geometry that is typically difficult to form, such as double curvature sections. An initial fabric blank size of 250x400mm, highlighted in Figure 3b, was selected to correspond with previous work using the same tool [12].

2.5. PREFORM DIGITISATION

The geometry of each preform was recorded using a Creaform Handyscan scanner with a scan resolution of 0.5mm. In-situ scanning within the DDF machine was conducted as opposed to stabilising the preform with a binder material and removing from the tool to both improve the rate at which preforms could be tested and to eliminate any uncontrolled relaxation of the preform. Additionally, the reduced reflectivity of the diaphragm material compared to the surface of the carbon fibre preform produced significantly higher quality scanning data. The workflow process of digitising a preform is shown in Figure 4. After the preform was stabilised, reflective markers required for scanning were applied to the upper diaphragm at regular intervals, as shown in Figure 4a. The form was then scanned in-situ, producing a point cloud and STL file for processing. The geometry was aligned to the principal axes using Creaform VX Elements scanning software, based on the centre of mass, producing a result such as the one shown in Figure 4b. The scan contained a portion of the tool surface, which was later used to assist with the alignment of the digital preform to the original geometry.

The 3D point cloud was processed using an iterative closest point algorithm in MATLAB to determine the distance of the surface preform from the original tool shape. Any data points in the lowest tenth percentile of the distances are considered to be part of the tool surface, rather than the preform, and are subsequently discarded. The contour plot shown in Figure 4c indicates each scanning point’s normal distance to the average thickness of the preform, which constitutes the wrinkle amplitude for this work. The wrinkle amplitude is therefore independent of the number of plies in the preform, enabling comparison between preforms of varying thicknesses.

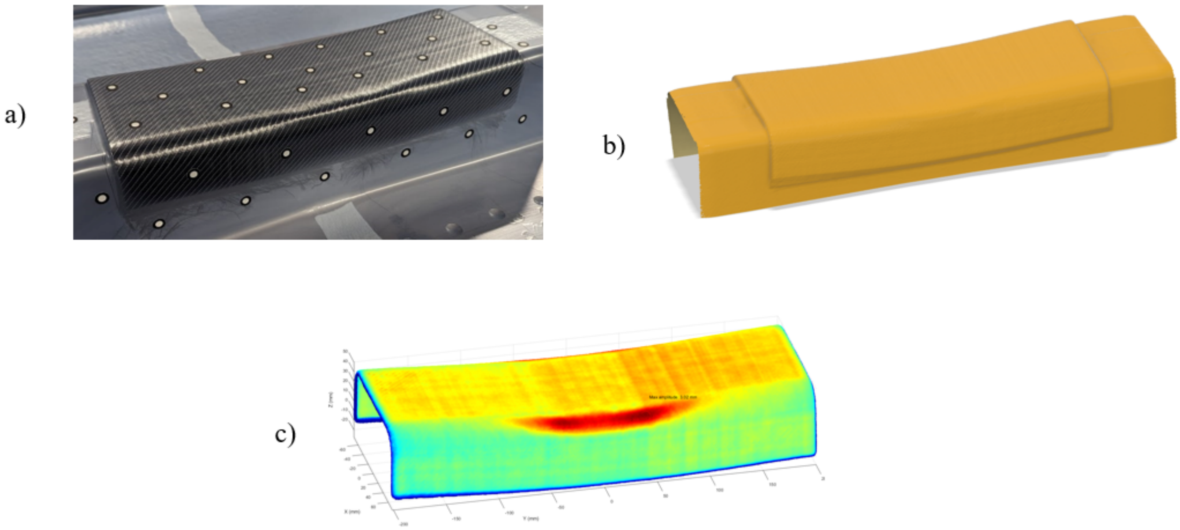

Figure 4 - Workflow for in-situ preform digitisation. a) Application of adhesive reflective points on the outer surface of the diaphragm. b) Raw scan result of the preform geometry using a 0.5mm resolution. c) Processed scan result of preform geometry, removing excess tool surface. Contour plot indicates difference from expected laminate thickness.

3. RESULTS

3.1. MULTI-PLY NON-LINEAR BENDING BEHAVIOUR

The bending stiffness of a single ply of FCIM359 is described by the bending moment versus curvature relationship shown in Figure 5a. The mean root mean square error (RMSE) between the fitted curve and the experimental data was found to be 4.2% and the results agreed well with previous bending characterisation of the same fabric [19]. The unstable behaviour observed in the low curvature regions of the bilinear bending moment align with data reported for textile materials in the literature [20]. Figure 5b describes the non-linear bending behaviour of a single ply of FCIM359, where the bending stiffness decreases as curvature increases. The initial bending stiffness at 0mm^{-1} curvature was found to be 0.0076Nm.

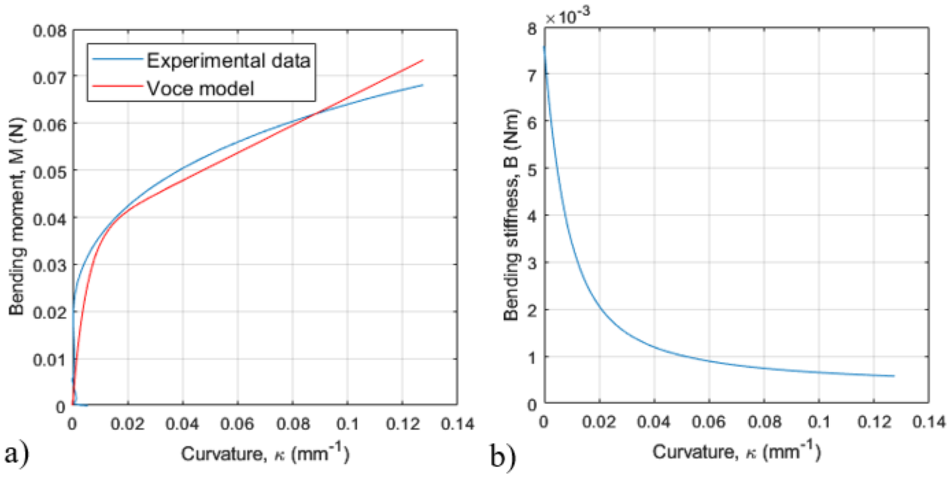

Figure 5a) Bending moment per unit width versus curvature for a single ply of FCIM359. b) Bending stiffness per unit width versus curvature for a single ply of FCIM359.

The multi-ply stack exhibited non-linear bending behaviour similar to the curves produced for a single ply. However, for samples of the same length, the multi-ply samples produced a smaller curvature range due to the resulting increased bending stiffness. The bending behaviour for a multiply stack is shown in Figure 6, where for a given curvature, the bending moment for a $[0/90]_{16}$ bending sample is greater than the summation of the bending moment for each individual ply in the stack. This difference is defined as the frictional moment (M_{Fric}), and has previously been observed by Liang et al. [13]. It is caused by the inter-ply friction in the laminate and is a significant component of the overall bending moment. This friction inhibits sliding between plies as they bend, effectively increasing the overall second moment of area of the system and subsequently increasing the perceived bending stiffness.

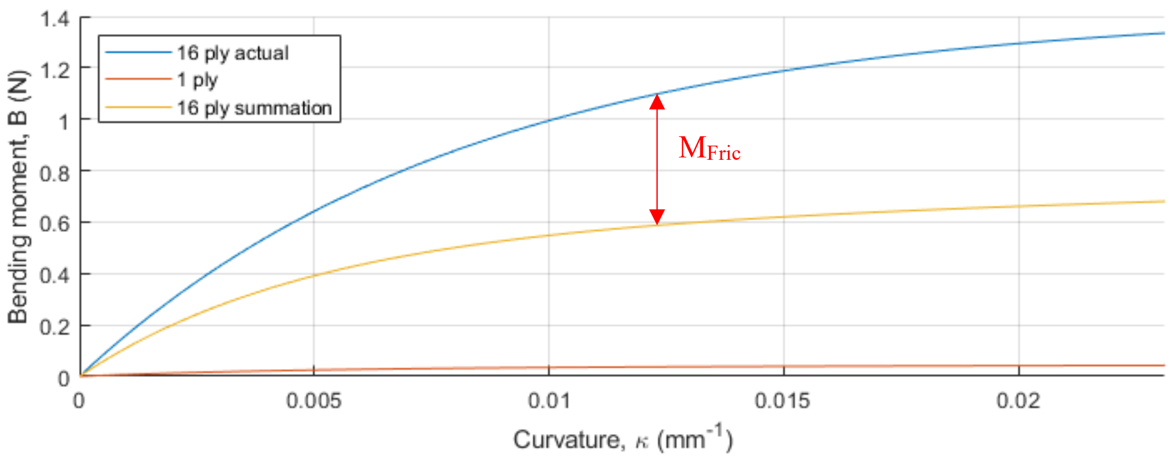

Figure 6 - Curvature-bending moment curves for a 16-ply sample, a 1-ply sample and a 16-ply summation of 1-ply.

Figure 7 shows the variation in the friction moment with curvature for the same 16-ply test (blue curve minus the yellow curve from Figure 6), which naturally also follows a non-linear relationship. The highest values of the friction moment can be seen when the curvature is at its largest, which occur at the tip of the laminate where the greatest levels of inter-ply slip are experienced and therefore the frictional forces are the greatest.

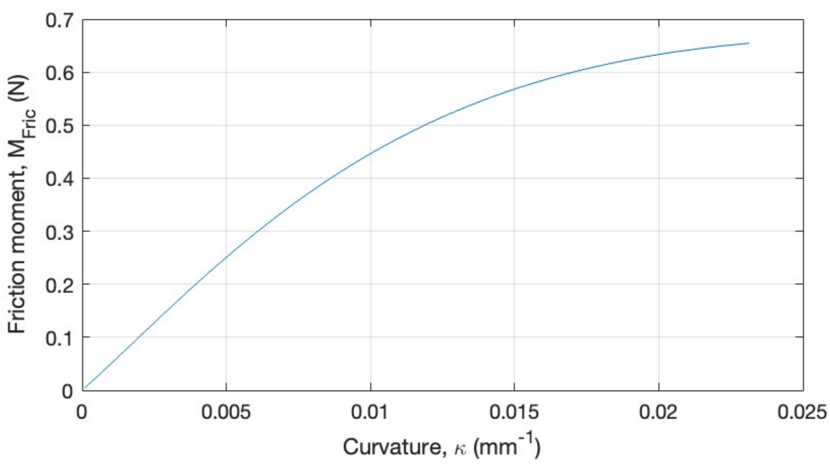

Figure 7 – Curvature versus friction moment for a 16-ply bending sample.

3.2. MULTI-PLY SHEAR BEHAVIOUR

Figure 8 shows the normalised shear force versus shear angle curves for a range of FCIM359 multi-ply layups, produced from the modified bias extension shear test. All curves represent the mean of a minimum of 3 repeats. The mean coefficients of variation were all found to be less than 1%, indicating good repeatability, and therefore error bars are omitted on Figure 8. The layup exhibiting the lowest shear resistance was found to be a $[\pm 45°]_8$ stack (green curve), which was subjected to atmospheric pressure only. The lack of normal compaction load limits inter-ply surface interactions, avoiding any significant resistance to the shear behaviour of the fabric. When vacuum pressure is introduced the shear resistance of the 8-ply stack (black line) is consistently higher. At an arbitrary shear angle of 20°, the shear force is 26.23% larger under the vacuum compaction load. This increase is likely caused by greater intra-ply friction between the yarns at the shear rotation points; as every ply is the same orientation, they are shearing in the same manner and slip between them is negligible.

The introduction of 8 additional [0°/90°] plies (denoted "16 ply" in Figure 8) exaggerates the influence of the inter-ply friction, which is dependent on the number of interfaces between plies of different orientations. It is assumed that the [0°/90°] plies do not shear and are relatively inextensible. The friction at these interfaces is therefore assumed to inhibit the shear deformation of the [±45°] plies, increasing the shear resistance of the laminate. A "blocked" layup of $[(0°/90°)_8, (\pm 45°)_8]$ only has a single inter-ply interface where the ply orientations are dissimilar. The small increase in shear force for any given shear angle produced (3% greater at a 20° shear angle) is greater than the mean coefficient of variation of either sample, indicating the increase is due to the introduction of the [0°/90°] material. Conversely, an "interleaved" layup of $[(0°/90°), (\pm 45°)]_8$ with 15 dissimilar ply-to-ply orientation interfaces produces very a high shear resistance curve, with a reported increase in shear force of 42% at a shear angle of 20° compared to the $[\pm 45°]_8$ layup.

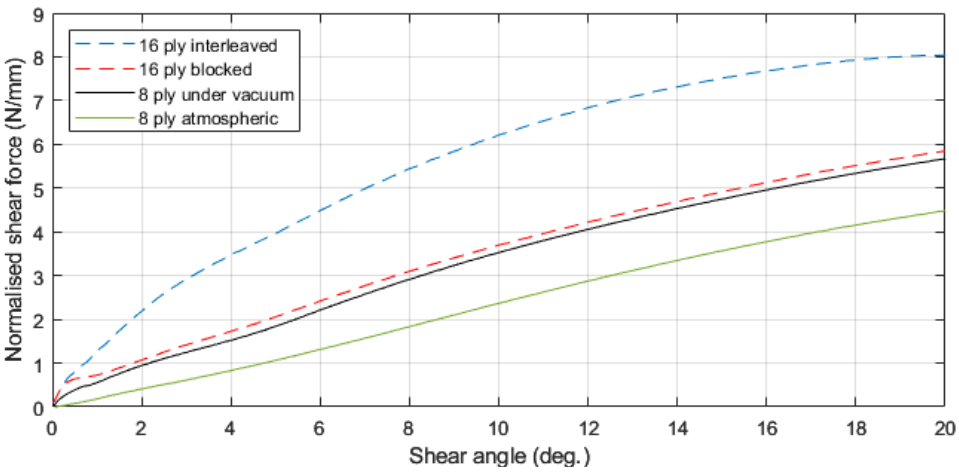

Figure 8 – Normalised shear force versus shear angle for a range of multi-ply FCIM359 layups.

3.3. DDF C-SPAR CASE STUDY

A DDF case study has been completed to investigate how the increased bending and shear stiffnesses caused by inter-ply friction influence the formability of thick laminates. Two independent variables have been studied: the total number of plies in the laminate, and the layup sequence. For each case, both [±45°] and [0°/90°] fabric blanks were used in every form.

Figure 9 shows the change in wrinkling pattern for the c-spar geometry as more plies are added to the stack, plus a graph indicating the associated increase in maximum wrinkle amplitude. When a [(0°/90°), (±45°)] 2-ply layup is formed, 2 transverse wrinkles are generated at the mid-section of the spar. Previous work [12] has concluded that these wrinkles are also a product of the constraints applied by inter-ply friction, as forms using single plies at both ply orientations do not produce any defects. These initial transverse wrinkles increase in amplitude and the distance between them increases when 4 plies are formed. Large longitudinal wrinkles begin to form on the external radii, and transverse wrinkles with a more severe amplitude appear in the centre of the spar. The maximum amplitude of these longitudinal wrinkles increases linearly as more plies are added to the laminate, up to an observed peak of 6.65mm for a total of 16 plies. The transverse wrinkles do not appear to increase in magnitude as the number of plies is increased.

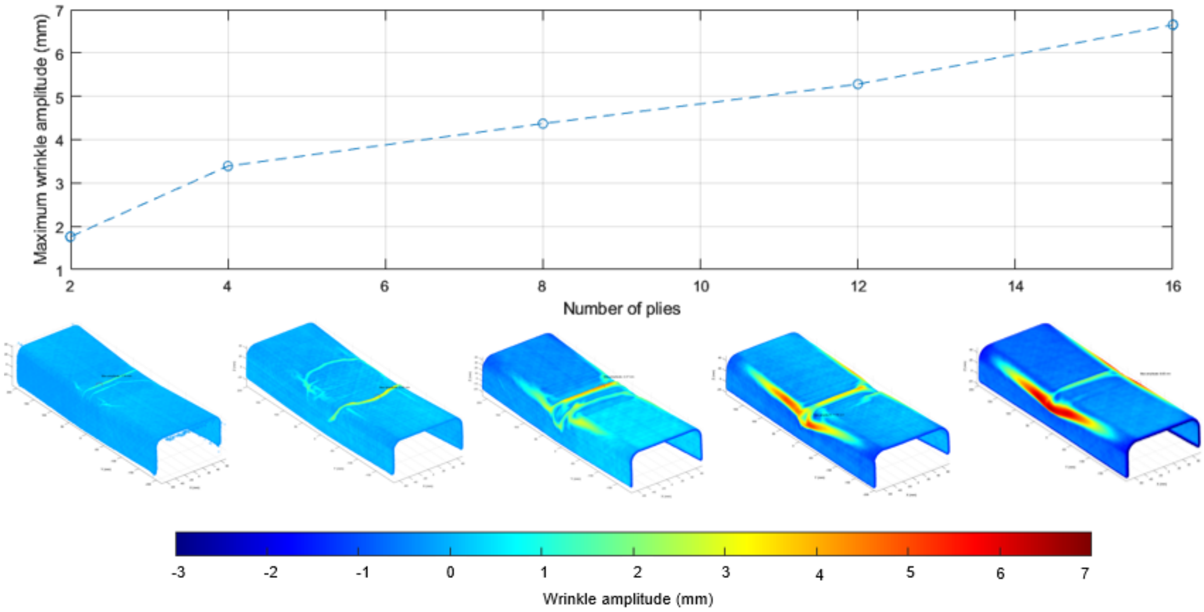

Figure 9 - Increase in maximum wrinkle amplitude with increasing total number of plies. Each laminate uses a [(0°/90°), (±45°)]$_n$ stacking sequence, where n ∈ (1, 2, 4, 6, 8).

Figure 10 shows how the amplitude in longitudinal wrinkles changes with respect to layup sequence. For this case study, 16 plies were used for every preform (8 plies at ±45° and 8 plies at 0°/90°). The layup sequence was changed in order to vary the number of slip interfaces between the two fibre orientations. For example, a [(0°/90°), (±45°)]$_8$ layup produces 15 slip interfaces as the orientations are entirely interleaved, whereas a [(0°/90°)$_4$, (±45°)$_8$, (0°/90°)$_4$] layup produces only 2 slip interfaces for the same number of plies. This enables layup sequences with 1, 2, 3, 7 or 15 possible slip interfaces for a 16-ply laminate. Figure 10 indicates how the maximum wrinkle amplitude appears to increase linearly before reaching a plateau, where increasing the number of slip interfaces produces no further increase in the wrinkle amplitude for the longitudinal wrinkles.

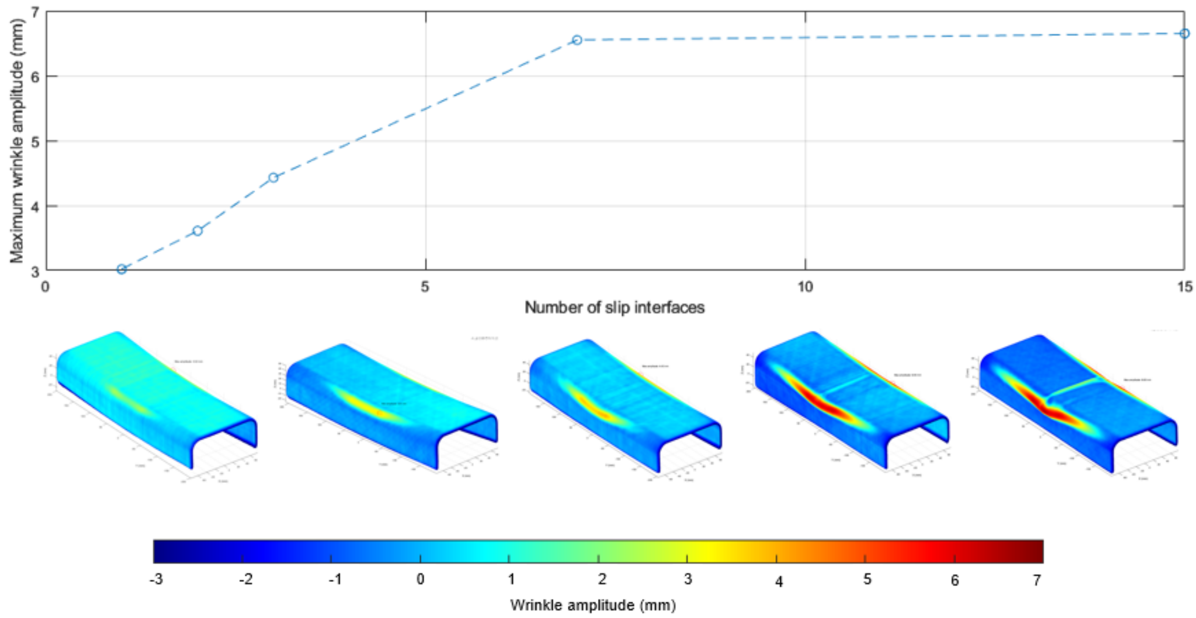

Figure 10 - Increase in maximum wrinkle amplitude with increasing number of slip interfaces. Each layup uses 8 plies at ±45° and 8 plies at 0°/90°, with varying layup sequences.

Whilst increased bending stiffness likely reduces the formability of the preform, the absence of longitudinal wrinkles when a $[0°/90°]_{16}$ laminate is formed suggests that the increased shear resistance is the dominant mechanism behind the formation of these longitudinal wrinkles. As the number of slip interfaces in the layup increases, the shear resistance within the stack increases due to high inter-ply friction. The shear resistance reaches a threshold level whereby the [±45°] plies cannot shear and must wrinkle out of plane to conform to the geometry. Once this threshold level has been reached, the magnitude of the out-of-plane wrinkle approaches a maximum, as very little shear is occurring. Additional trials (not currently presented) showed that lubricating the plies with uncured epoxy resin or heat-activated powder binder reduced the inter-ply coefficient of friction sufficiently to enable greater intra-ply shear, eliminating the longitudinal wrinkles. Likewise, the reduced constraints of single diaphragm forming (SDF) produced interleaved preforms without wrinkles, as the inter-ply friction was less significant.

4. CONCLUSIONS AND FUTURE WORK

Inter-ply friction can have a significant influence on the deformation mechanisms required to form multi-ply NCF preforms. The bending behaviour of a multi-ply preform has been demonstrated to be non-linear, and inter-ply friction contributes a considerable proportion to the overall bending moment. Inter-ply friction also has a significant impact on the intra-ply shear behaviour of a multi-ply laminate. The shear resistance of a fabric stack is increased when constrained by fabric-fabric friction, and the number of shear to non-shear fabric interfaces dominates this behaviour. Finally, a DDF case study has been presented demonstrating the severe reduction in formability caused by the increased multi-ply shear resistance.

Future work will evaluate the relative contributions from the bending stiffness and shear resistance on the formability of a preform. Additionally, drawbacks of the characterisation tests presented will be addressed, such as a more accurate measurement of shear angle and checking for any distortion of the interleaved [0°/90°] fabric in the bias extension test, using digital image correlation.

ACKNOWLEDGEMENTS

This work was funded by the Engineering and Physical Sciences Research Council [Grant number: EP/P006701/1], as part of the "EPSRC Future Composites Manufacturing Research Hub". Access to the 3D laser scanner was kindly provided by the HV-Command EPSRC Strategic Equipment Grant (EP/T006420/1) at the University of Nottingham.

REFERENCES

1. Yu F, Chen S, Harper LT, Warrior NA. Double diaphragm forming simulation using a global-to-local modelling strategy for detailed defect detection in large structures. Compos Part A Appl Sci Manuf. 2021;147(April).
2. Thompson AJ, Belnoue JPH, Hallett SR. Modelling defect formation in textiles during the double diaphragm forming process. Compos Part B Eng. 2020;202(July):108357.
3. Alshahrani H, Hojjati M. Experimental and numerical investigations on formability of out-of-autoclave thermoset prepreg using a double diaphragm process. Compos Part A Appl Sci Manuf. 2017; 101:199–214.
4. Sun J, Gu Y, Li M, Ma X, Zhang Z. Effect of forming temperature on the quality of hot diaphragm formed C-shaped thermosetting composite laminates. J Reinf Plast Compos. 2012;31(16):1074–87.
5. Potter K, Khan B, Wisnom M, Bell T, Stevens J. Variability, fibre waviness and misalignment in the determination of the properties of composite materials and structures. Compos Part A Appl Sci Manuf. 2008;39(9):1343–54.
6. Bel S, Boisse P, Dumont F. Analyses of the deformation mechanisms of non-crimp fabric composite reinforcements during preforming. Appl Compos Mater. 2012;19(3–4):513–28.
7. Viisainen J V., Hosseini A, Sutcliffe MPF. Experimental investigation, using 3D digital image correlation, into the effect of component geometry on the wrinkling behaviour and the wrinkling mechanisms of a biaxial NCF during preforming. Compos Part A Appl Sci Manuf. 2021;142(October 2020):106248.
8. Chen S, McGregor OPL, Harper LT, Endruweit A, Warrior NA. Defect formation during preforming of a bi-axial non-crimp fabric with a pillar stitch pattern. Compos Part A Appl Sci Manuf. 2016;91:156–67.
9. Chen S, McGregor OPL, Endruweit A, Elsmore MT, De Focatiis DSA, Harper LT, et al. Double diaphragm forming simulation for complex composite structures. Compos Part A Appl Sci Manuf. 2017;95:346–58.
10. Yu F, Chen S, Viisainen J V., Sutcliffe MPF, Harper LT, Warrior NA. A macroscale finite element approach for simulating the bending behaviour of biaxial fabrics. Compos Sci Technol. 2020;191(October 2019).
11. Lawrence GD, Chen S, Warrior NA, Harper LT. The influence of inter-ply friction during double-diaphragm forming of biaxial NCFs. Compos Part A Appl Sci Manuf. 2023;167(January):107426.
12. Yu F, Chen S, Harper LT, Warrior NA. Investigation into the effects of inter-ply sliding during double diaphragm forming for multi-layered biaxial non-crimp fabrics. Compos Part A Appl Sci Manuf. 2021;150(May).
13. Liang B, Colmars J, Boisse P. A shell formulation for fibrous reinforcement forming simulations. Compos Part A Appl Sci Manuf. 2017;100:81–96.
14. de Bilbao E, Soulat D, Hivet G, Gasser A. Experimental Study of Bending Behaviour of

Reinforcements. Exp Mech. 2010;50(3):333–51.

15. Bouquerel L, Moulin N, Drapier S, Boisse P, Beraud JM. Modelling and simulating the forming of new dry automated lay-up reinforcements for primary structures. In: AIP Conference Proceedings. 2017.
16. Cao J, Akkerman R, Boisse P, Chen J, Cheng HS, de Graaf EF, et al. Characterization of mechanical behavior of woven fabrics: Experimental methods and benchmark results. Compos Part A Appl Sci Manuf. 2008;39(6):1037–53.
17. Alshahrani H, Hojjati M. Influence of double-diaphragm vacuum compaction on deformation during forming of composite prepregs. J Sci Adv Mater Devices. 2016;1(4):507–11.
18. Johnson KJ, Butler R, Loukaides EG, Scarth C, Rhead AT. Stacking sequence selection for defect-free forming of uni-directional ply laminates. Compos Sci Technol. 2019;171:34–43.
19. Yu F, Chen S, Viisainen J V., Sutcliffe MPF, Harper LT, Warrior NA. A macroscale finite element approach for simulating the bending behaviour of biaxial fabrics. Compos Sci Technol. 2020;191(January).
20. Broberg PH, Lindgaard E, Krogh C, Jensen SM, Trabal GG, Thai AF. One-click bending stiffness : Robust and reliable automatic calculation of moment – curvature relation in a cantilever bending test. Compos Part B. 2023;260(November 2022):110763.